

THE SOLAR WIND ENVIRONMENT IN TIME

QUENTIN POGNAN¹, CECILIA GARRAFFO¹, OFER COHEN^{2,1}, JEREMY J. DRAKE¹¹Harvard-Smithsonian Center for Astrophysics, 60 Garden St. Cambridge, MA 02138²Lowell Center for Space Science and Technology, University of Massachusetts, Lowell, MA 01854, USA

ABSTRACT

We use magnetograms of 8 solar analogues of ages 30 Myr to 3.6 Gyr obtained from Zeeman Doppler Imaging (ZDI) and taken from the literature, together with two solar magnetograms, to drive magnetohydrodynamical (MHD) wind simulations and construct an evolutionary scenario of the solar wind environment and its angular momentum loss rate. With observed magnetograms of the radial field strength as the only variant in the wind model, we find that power law model fitted to the derived angular momentum loss rate against time, t , results in a spin down relation $\Omega \propto t^{-0.51}$, for angular speed Ω , which is remarkably consistent with the well-established Skumanich law $\Omega \propto t^{-0.5}$. We use the model wind conditions to estimate the magnetospheric standoff distances for an Earth-like test planet situated at 1 AU for each of the stellar cases, and to obtain trends of minimum and maximum wind ram pressure and average ram pressure in the solar system through time. The wind ram pressure declines with time as $\overline{P_{ram}} \propto t^{2/3}$, amounting to a factor of 50 or so over the present lifetime of the solar system.

Keywords: stars: rotation — stars: magnetic field — stars: evolution — stars: stellar winds — stars: solar like

1. INTRODUCTION

As with all stars, the Sun has undergone significant changes during its lifetime. In addition to the substantial structural changes from its pre-main sequence phase through to evolution on the main-sequence (e.g. Sagan & Mullen 1972; Cox & Guzik 1995; Boothroyd & Sackmann 2003), its rotation and associated magnetic activity have also changed quite radically (e.g. Güdel 2007; Guinan & Engle 2009). Understanding the Sun's past is of fundamental importance for understanding the solar system as a whole. Changes in radiative energy, magnetic field, the solar wind and more transient phenomena such as flares and coronal mass ejections have inevitably played a major role in planetary evolution and the appearance of life on Earth. Realisation has been growing that the Sun's magnetic activity is particularly important. It is the source of UV–X-ray radiation that would likely have driven significant mass loss from planetary envelopes early in solar system history (Owen & Wu 2016), and of the solar wind thought to be the culprit behind the disappearance of water from Mars during the Noachian period (e.g. Terada et al. 2009). The solar wind is also the driving force behind the heliospheric bubble that has protected the solar system from potentially harmful cosmic rays, both today and during the epoch of emergent life on Earth (Cohen et al. 2012).

The magnetic activity of a star is dependent on its

magnetic dynamo, which in turn harbours a strong relation with the rotation period of the star (e.g. Skumanich 1972; Pallavicini et al. 1981; Wright & Drake 2011). In accordance with main sequence development, the Sun is thought to have been rotating much faster in its younger days by up to 10 times or so (Guinan & Engle 2009), which would have induced a much more vigorous dynamo and stronger magnetic activity (e.g. Güdel 2007). This implies a significantly different solar environment in the past than the present day one.

Magnetized stellar winds cause mass and angular momentum loss when they break away from the star's magnetic field in a process called magnetic braking (Schatzman 1962; Weber & Davis 1967; Mestel 1968; Mestel & Spruit 1987). It is theorised that these winds are driven by magnetic processes ultimately powered by the stellar magnetic dynamo. Although the exact physics involved has not been unequivocally identified, dissipation of Alfvén wave pressure (Belcher 1971) is gaining widespread acceptance as a dominant mechanism (e.g. Suzuki 2006; Cranmer & van Ballegoijen 2005; van Ballegoijen et al. 2011).

Since the dynamo has an intrinsic link to the star's rotation period, it is also related to the age of the star. It is known that stellar rotation rates, Ω , eventually converge to the empirically observed Skumanich Law, $\Omega \sim t^{-1/2}$ (Skumanich 1972). However the relation is not very well

understood for the early stages of stellar evolution. Recent surveys of young open clusters (e.g. Meibom et al. 2011) have found a wide range of rotation periods for younger stars. Thus it is a safe assumption that the Sun must have had very different angular braking and mass loss rates during its earlier lifetime.

In order to understand how the Sun behaved in past stages of its life we can look to similar but younger solar analogue stars (Güdel 2007; Guinan & Engle 2009; Ribas et al. 2005, 2010) which can provide insight into the solar environment at earlier times. With some understanding of the powering of the present day solar wind by the surface magnetic field, observations of the magnetic fields of solar analogues can also be used to attempt to constrain the Sun’s stellar wind environment at various points in its life (see, e.g., Sterenborg et al. 2011, for a proof of concept example). Current space weather models (e.g. Cohen et al. 2008) utilize detailed solar magnetograms obtained using Michelson Doppler Imaging (MDI) (Scherrer et al. 1995) as the lower magnetic field boundary condition. With recent developments in instrumentation and observational techniques, one of the most powerful methods for acquiring magnetic field data on other late-type stars is Zeeman Doppler Imaging (ZDI; see, e.g., Brown et al. 1991; Donati & Brown 1997; Hussain et al. 2009) from which large-scale magnetograms of stellar surfaces can be retrieved.

In this study, we look at solar analogues of various ages as proxies for the Sun in its youth. We present the results of numerical simulations in the solar coronal regime for 8 solar-type stars with ages ranging from 30 Myr to 3.6 Gyr. From the models we extract the rates for mass and angular momentum losses of each star, as well as the range of wind speeds and associated densities. The wind speeds and densities are extrapolated from 1 Au up to 100 AU to examine the ram pressures at distances comparable to those of solar system planets from the Sun. Notably the 1 Au distance is used to calculate magnetospheric standoff radii to examine the consequent implications for the terrestrial magnetosphere. We also make use of two solar magnetograms, one with high resolution and the other with resolution closer to that of the ZDI maps, in order to test the effects of limited magnetogram resolution obtained from the ZDI approach.

We begin by detailing the numerical magnetohydrodynamics (MHD) simulations in Section 2. We then present the results of the modeling in Section 4 and discuss the main findings in Section 5. We finish with Section 6, where we conclude that the use of ZDI magnetograms of solar analogues is a valid method for studying the Sun’s past and should be continued with the advent of future data.

2. MHD NUMERICAL SIMULATION

The numerical solutions discussed in this paper are obtained using the generic *BATS-R-US* code (Powell et al. 1999), which is a part of the Space Weather Modelling Framework (SWMF Tóth et al. 2012). The SWMF is a collection of physics-based models which work in different regimes of solar and space physics. The results presented in this paper make use of the solar corona (SC) component (see van der Holst et al. 2014). To obtain these results, we use the code to solve a set of 3D MHD equations for loss of angular momentum and mass. Other parameters such as maximum and minimum radial wind velocities and their associated densities are also extracted. The SC module uses maps of the radial magnetic field of the source to specify the field boundary conditions (see Cohen et al. 2008; Alvarado-Gómez et al. 2016, for details) at the surface of the star. These maps are obtained using ZDI, which allows large scale magnetic topology to be recovered (e.g. Donati & Brown 1997; Hussain et al. 2009). This method has been thoroughly tested and found to recover the general field distribution of solar-like stars (Donati et al. 2008; Petit et al. 2008; Alvarado-Gómez et al. 2015; Hussain et al. 2016), thus making it a reliable provider of magnetic field maps for the SWMF SC module. We also use a high resolution solar magnetogram obtained using MDI (see Scherrer et al. 1995) from publicly available Stanford data¹, and a low resolution magnetogram obtained from the Wilcox Solar Observatory (WSO)². Both solar magnetograms were taken during the same solar maximum on April 19th 2000.

Once the SC module is provided with the ZDI magnetogram, a field potential extrapolation above the stellar surface is conducted and is used as the initial conditions for the simulation. The solar corona is taken to start at the base of the chromosphere and extends generally up to around $40R_*$, though this distance can be larger for stars with strong magnetic fields. The SC module also requires input of stellar parameters radius R_* , mass M_* and rotation period P_{rot} , as well as the chromospheric base density n_0 and temperature T_0 . The stellar parameters are obtained from the same papers as the magnetograms, or failing that are taken to be solar values. The coronal base density and temperature are taken to be solar values: $n_0 = 2.0 \times 10^8 \text{ cm}^{-3}$ and $T_0 = 1.5 \times 10^6 \text{ K}$. This assumption allows for easier comparison between the solar analogues and the two solar magnetograms and should be a reasonable approxima-

¹ <http://hmi.stanford.edu/data/synoptic.html>

² <http://wso.stanford.edu/>

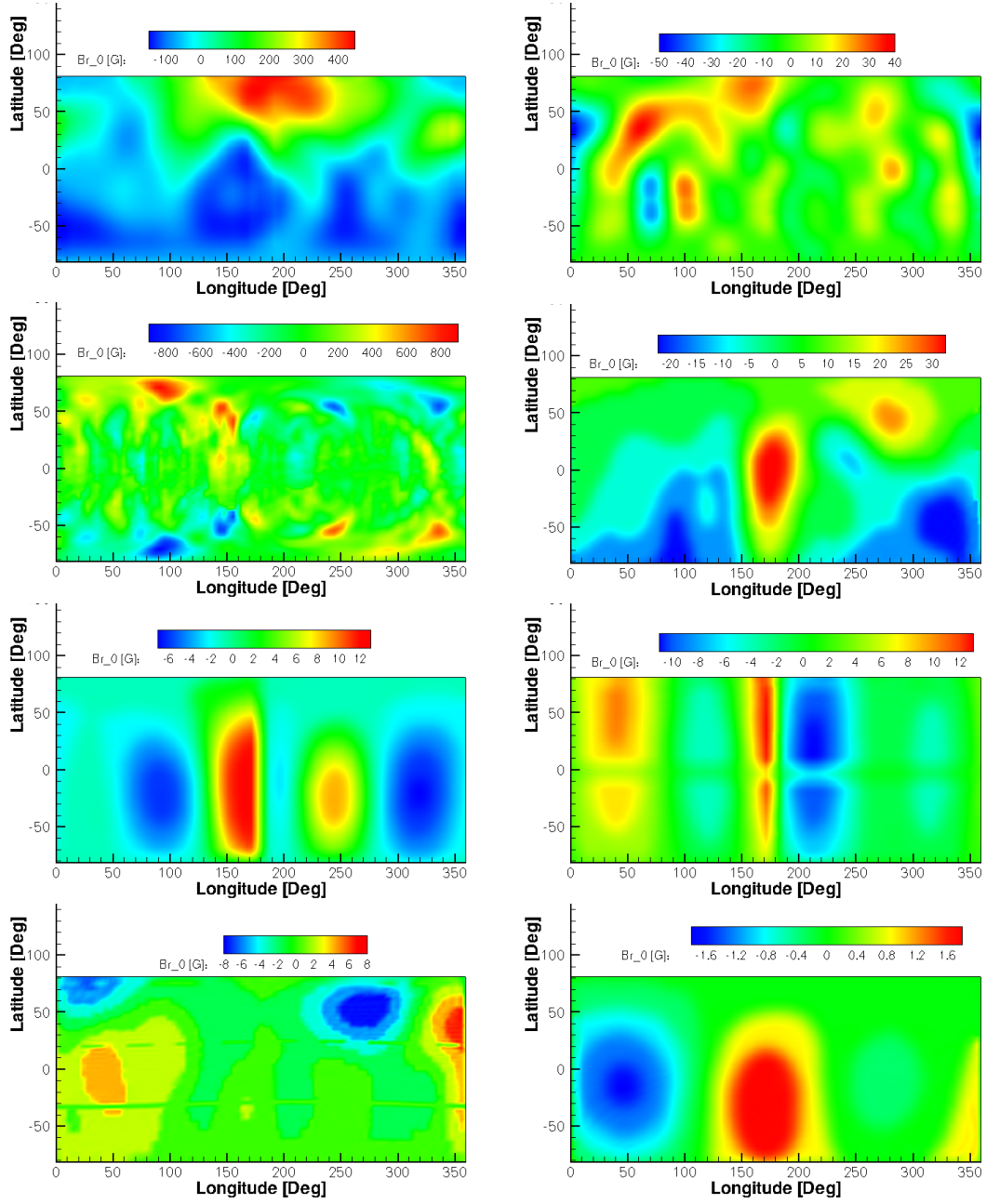


Figure 1. Magnetograms of the solar analogues in order of ascending age from top left to bottom right: HD 29615, HD 35296, AB Dor, HD 206860, HD 73350, HD 73256, Tau Boo, HD 76151

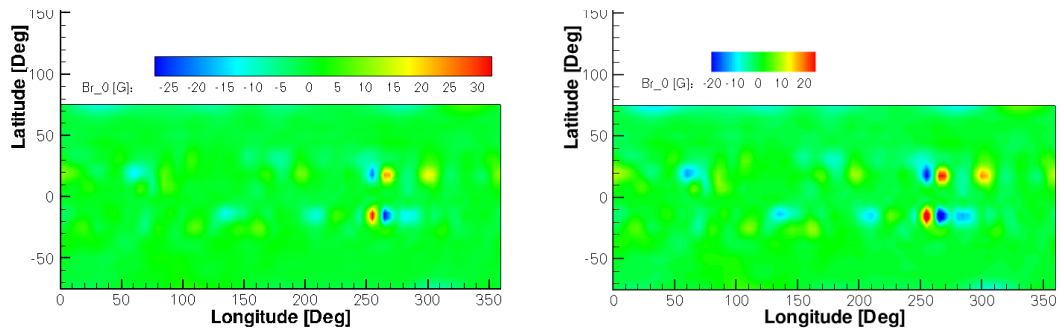


Figure 2. High and low resolution solar magnetograms. High resolution was obtained from <http://hmi.stanford.edu/data/synoptic.html> and low resolution from <http://wso.stanford.edu>. Note the different scales.

tion since all the stars in this sample are solar-like and well below X-ray saturation.

We use a spherical three-dimensional grid with a logarithmic scale in the \hat{r} direction. With the magnetic field initial conditions provided by the magnetogram, the program evolves the coronal heating and stellar winds self-consistently using Alfvén wave dissipation through a turbulent energy cascade. Processes such as electron heat conduction and radiative cooling are also taken into account (see [Oran et al. 2013](#); [Sokolov et al. 2013](#); [van der Holst et al. 2014](#), for details). We conduct three-dimensional simulations for eight solar-like stars and two solar cases, the magnetograms for which can be seen in Figures 1 and 2. The parameters and sources of the magnetograms can be found in Table 1.

The simulation provides a three-dimensional solution of the stellar corona, from which we extract the wind density ρ , and the maximum and minimum radial velocities, U_R^{max} and U_R^{min} . This is defined as the region of the outer solar corona where the winds speeds are greater than the Alfvén speed, $v_A = B/\sqrt{4\pi\rho}$, where B is defined as $B = \sqrt{B_x^2 + B_y^2 + B_z^2}$ and ρ is the mass density for a pure hydrogen wind with the electron contribution neglected. The super-Alfvénic region is conveniently visualised as the volume exterior to the Alfvén Surface, itself defined as the collection of points in space at which the ratio of wind speed to local Alfvén speed is unity: $M_A = U/v_A = 1$. We find the total angular momentum and mass loss rates by integrating the loss rates over the entire surface. Equations 1 and 2 give the rates for mass and angular momentum loss respectively:

$$\frac{dM}{dt} = \rho(\mathbf{u} \cdot d\mathbf{A}) \quad (1)$$

$$\frac{dJ}{dt} = \Omega \rho R^2 \sin^2 \theta (\mathbf{u} \cdot d\mathbf{A}), \quad (2)$$

where $d\mathbf{A}$ is the surface element on the Alfvén Surface and dJ/dt is the component of the angular momentum change in the direction of the rotation axis. We take dJ/dt to be the only angular momentum component contributing to a change in the magnitude of J . From dJ/dt we may also find the spin down evolution using:

$$\frac{dJ}{dt} = I \frac{d\Omega}{dt}, \quad (3)$$

where I is the moment of inertia and Ω is the angular frequency. Integrating a power law fit to dJ/dt will allow a relation for Ω as a function of time to be obtained and compared to the Skumanich Law. We take the moment of inertia of solar like stars to be $I = 0.076MR^2$ ([Claret & Gimenez 1989](#)) and constant in time.

We also find the range of wind speed and density at a distance of 1 AU from the star, in order to study the effect of ram pressure on a magnetosphere with a magnetic

field similar to that of a young Earth’s or a similarly placed planet around a solar analogue. A maximum and minimum wind speed and their associated densities are found within the stellar corona solution, in the super-Alfvénic region. As the wind speeds asymptotically approach a maximum at the Alfvén Surface, the maximum and minimum found in the stellar corona solution in the super-Alfvénic region can be used directly for the 1 AU distance. The corresponding densities are extrapolated following a $1/R^2$ law. In order to find an approximate range of values for the ratio of the size of a test planet’s magnetosphere to the planet’s radius, we equate wind ram pressure to the magnetic pressure of the planetary field and rearrange to get the usual relation for the magnetosphere standoff distance when the wind magnetic pressure can be neglected:

$$\frac{R_{Mp}}{R_p} = \left(\frac{2B_p^2}{\mu_0 \rho U_R^2} \right)^{\frac{1}{6}} \quad (4)$$

where μ_0 is the permeability of free space and B_p is the equatorial magnetic field strength at the planet’s surface. We also extrapolate ram pressure up to 100 Au for a range of stellar ages, in order to give a clear visual of the decline of ram pressure over time.

3. STELLAR SAMPLE

We use a sample of 8 solar-like stars and 2 solar magnetograms of different resolutions to conduct our investigation. The stellar parameters and magnetogram sources are described in brief in table 1, and individually in more detail in the following subsections. While our sample contains a range of spectral types from F7 to K0, our assumption is that we can use the model honed to match the observed solar wind for any star with a hot corona for which the stellar wind is accelerated in a similar manner to the solar wind ([Cohen et al. 2010a, 2012](#)). This is in contrast to, for example, line driven winds in giant stars (see e.g. [Airapetian et al. \(2003\)](#); [De Beck et al. \(2010\)](#)). Our model assumes coronal heating and wind acceleration via Alfvén wave dissipation, while also taking into account the scaling of the magnetic flux with X-ray flux ([Pevtsov et al. 2003](#)) via the Poynting flux providing the energy to the corona. This implementation accounts, at least in part, for the affect of different convection zone parameters on the coronal heating and wind acceleration. The latter relation is worthy of further study, though falls beyond the scope of the present work.

3.1. HD 29615

HD 29615 is a G3V type star of age 30_{-10}^{+10} Myr ([Zuckerman & Song 2004](#); [Waite et al. 2015](#)) with a rotation

Table 1. Parameters of stellar sample and magnetogram sources.

Star	Spectral Type	Age (Gyr)	P_{rot} (days)	$Log(L_X)^b$ ($erg/s/cm^2$)	ZDI Ref.
HD 29615	G3V	$0.03^{+0.01}_{-0.01}$	$2.34^{+0.02}_{-0.05}$		1
HD 35296	F8V	$0.04^{+0.01}_{-0.01}$	$3.48^{+0.01}_{-0.01}$	29.33	1
AB Doradus	K0V	$0.075^{+0.025}_{-0.025}$	$0.5^{+0.1}_{-0.1}$	30.33	2
HD 206860	G0V	$0.25^{+0.05}_{-0.05}$	$4.6^{+0.1}_{-0.1}$	29.19	3
HD 73350	G5V	$0.80^{+0.30}_{-0.30}$	$12.3^{+0.1}_{-0.1}$	28.72	4
HD 73256	G8	$0.83^{+0.03}_{-0.03}$	$14.0^{+0.1}_{-0.1}$		5
τ Boötis	F7V	$2.4^{+0.7}_{-1.1}$	$3.0^{+0.1}_{-0.1}$	28.85	6
HD 76151	G3V	$3.6^{+1.8}_{-2.3}$	$20.5^{+0.3}_{-0.3}$	28.40	4
Sun (high res) ^a	G2V	$4.57^{+0.01}_{-0.01}$	$25.5^{+0.01}_{-0.01}$	27.3 ^c	7
Sun (low res) ^a	G2V	$4.57^{+0.01}_{-0.01}$	$25.5^{+0.01}_{-0.01}$	27.3 ^c	8

References—(1) [Waite et al. \(2015\)](#); (2) [Hussain et al. \(2007\)](#); (3) [Boro Saikia et al. \(2015\)](#); (4) [Petit et al. \(2008\)](#); (5) [Fares et al. \(2013\)](#); (6) [Fares et al. \(2009\)](#); (7) <http://hmi.stanford.edu/data/synoptic.html>; (8) <http://wso.stanford.edu/>

^aCorresponding to the solar maximum of 2000 April 19.

^bX-ray flux from <http://www.hs.uni-hamburg.de/DE/For/Gal/Xgroup/nexus/index.html>

^cFrom [Gudel et al. \(1996\)](#)

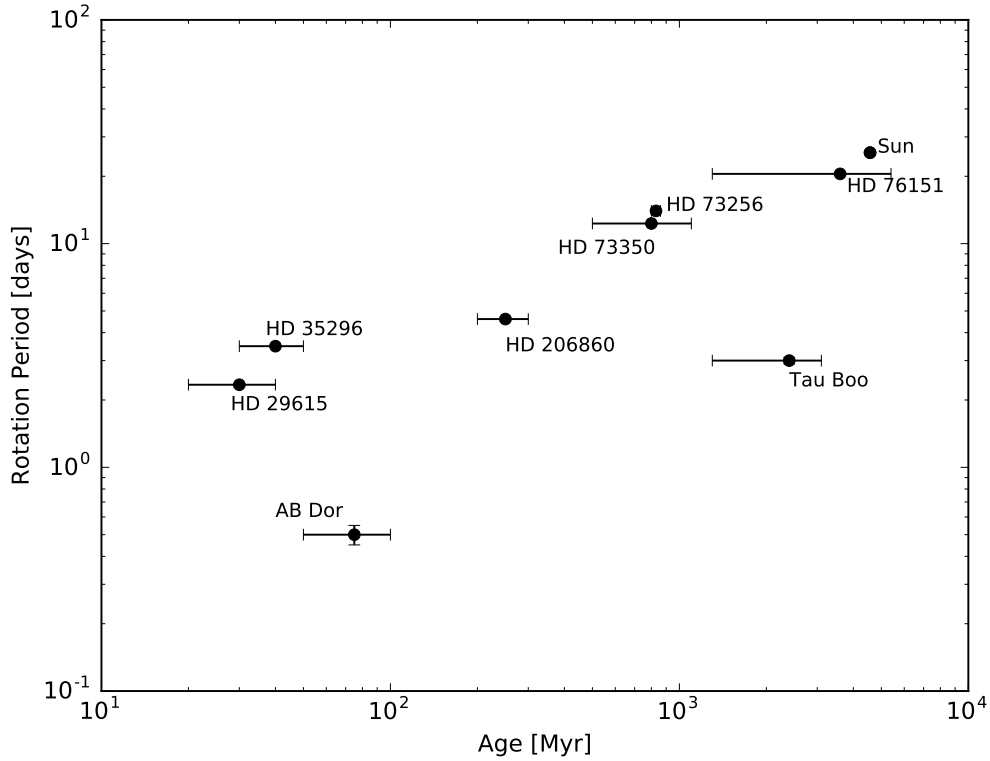


Figure 3. Plot of rotation period as a function of age for the stars in our sample. Note that the error bars for rotation period are too small to be seen.

period of $2.34^{+0.02}_{-0.05}$ days (Waite et al. 2015).

3.2. HD 35296

HD 35296 is a F8V type star of age 40^{+10}_{-10} Myr, with a rotation period of $3.48^{+0.01}_{-0.01}$ days (Waite et al. 2015).

3.3. AB Dor

AB Dor is a K0 dwarf (Torres et al. 2006) of age 50 Myr, with a rotation period of $0.5^{+0.1}_{-0.1}$ days (Hussain et al. 2007; Plavchan et al. 2009). While it is clear that AB Dor must be a young star, the exact age is subject to some uncertainty. We adopt the value of 75^{+25}_{-25} Myr (Zuckerman & Song 2004; Plavchan et al. 2009) as a fairly conservative estimate and range. There is some debate as to whether AB Dor is a pre-main sequence star or if it has just arrived on the main sequence (Hussain et al. 2007). While differing in spectral type from the Sun more than the other stars of the study, AB Dor still represents the most well-studied rapidly rotating solar-like star, especially in regard to surface magnetic field distribution, activity and winds (see, e.g., Hussain et al. (2007); Donati et al. (2009); Cohen et al. (2010b)).

3.4. HD 206860

HD 206860 (also known as HN Peg) is a G0 type star of age 200 Myr, with a rotation period of $4.6^{+0.1}_{-0.1}$ days (Pizzolato et al. 2003; Boro Saikia et al. 2015). There has been some matter of debate over the true age of HD 206860. Luhman et al. (2007) give an age of 300 Myr, while Barnes (2007) finds 247^{+42}_{-42} Myr using gyrochronology. We decide to take a conservative middle ground and use 250^{+50}_{-50} Myr as HD 206860's age.

3.5. HD 73350

HD 73350 is a G5 type star with a rotation period of $12.3^{+0.1}_{-0.1}$ days (Petit et al. 2008; Vidotto et al. 2014). HD 73350 was originally thought to be quite an old star only slightly younger than the Sun, with an age of $4.1^{+2.0}_{-2.7}$ Gyr (Valenti & Fischer 2005), but more recent studies have observed a debris disk, yielding a much younger age of 513^{+136}_{-136} Myr (Plavchan et al. 2009). **However, this appears to be an underestimation, as a recent survey of the Hyades cluster (~ 800 Myr) has found similar G5 stars with rotation periods of ~ 10 -11 days (Douglas et al. 2016). In order to accurately reflect the uncertainty in this star's age, we take a value of 800^{+300}_{-300} Myr.**

3.6. HD 73256

HD 73256 is a G8 type star of age 830^{+30}_{-30} Myr (Udry et al. 2003; Saffe et al. 2005; Fares et al. 2013) with a rotation period of $14.0^{+0.1}_{-0.1}$ days (Udry et al. 2003; Fares et al. 2013). It should be noted that HD 73265 has a hot Jupiter orbiting it with a period of about 2.55 days at

a distance of 0.37 Au (Udry et al. 2003). It is possible that the presence of a close-in hot Jupiter may affect the stellar activity properties through influence on rotation, though no evidence of tidal effects have been seen, and the stellar rotation and planet orbital periods are very different.

3.7. τ Boötis

τ Boötis is a F7 type star of age 2.4 Gyr (Saffe et al. 2005; Mamajek & Hillenbrand 2008), with a rotation period of $3.0^{+0.1}_{-0.1}$ days (Fares et al. 2009). τ Boötis' age has also been hotly debated, and is often cited to be anywhere between 1.3-3.1 Gyr (e.g. Fuhrmann et al. 1998; Borsa et al. 2015); we chose to use $2.4^{+0.7}_{-1.1}$ Gyr. Furthermore, τ Boötis hosts a hot Jupiter with an orbital period of 3.3 days (Butler et al. 1997; Catala et al. 2007; Donati et al. 2008; Fares et al. 2009). Donati et al. (2008) even suggest that "the tidal effects induced by the giant planet can be strong enough to force the thin convective envelope into corotation." Thus, while we include τ Boötis in our sample as we still believe the wind producing mechanism is solar like, the MHD simulation results for this star should be taken as potentially less reliable than for the rest of the sample.

3.8. HD 76151

HD 76151 is a G3 type star of age $3.6^{+1.8}_{-2.3}$ Gyr (Valenti & Fischer 2005; Vidotto et al. 2014), with a rotation period of $20.5^{+0.3}_{-0.3}$ days (Petit et al. 2008; Vidotto et al. 2014).

3.9. Sun

The Sun is a G2 type star of age $4.57^{+0.01}_{-0.01}$ Gyr, with a rotation period of $25.5^{+0.1}_{-0.1}$ days (Bonanno et al. 2002; Pizzolato et al. 2003; Connelly et al. 2012). While the underlying magnetic morphology of the Sun is normally a dipole, this is not the case during a solar maximum such as that of April 2000 when our two solar magnetograms were taken.

4. RESULTS

We present the results for the solar analogues in section 4.1, including a look at their age-rotation trend (Figure 3) as well as their average surface magnetic fields with respect to age and rotation period (Figure 4). We also look at the mass and angular momentum loss rates (Figures 5 and 6) and calculate a range of possible magnetosphere sizes for a sample planet with a 0.3G equatorial field (Figure 8). Ram pressures are also extrapolated up to 100 Au for locii of different ages (Figure 9). In Section 4.2 we look at the results from the two solar magnetograms, and compare these to the ones obtained from the solar analogues. Three-dimensional

Table 2. Calculated quantities from MHD simulations

Star	$\langle B \rangle^b$ (G)	dM/dt^c ($10^{-14} M_{sol}/yr$)	dJ/dt^d (erg)	$\rho(U_R^{max})^2$ ($10^{-8} dyn cm^{-2}$) ^e	$\rho(U_R^{min})^2$ ($10^{-8} dyn cm^{-2}$) ^e
HD 29615	6.85E1	9.50	4.69E31	23.6	42.9
HD 35296	7.16	3.18	3.00E31	4.42	5.77
AB Doradus	1.19E2	12.5	2.15E33	43.5	48.1
HD 206860	6.64	2.27	2.57E31	7.07	10.9
HD 73350	2.45	1.10	2.53E30	1.28	2.82
HD 73256	2.96	0.745	1.26E30	7.16	5.72
τ Boötis	1.26	0.933	1.19E31	2.07	1.45
HD 76151	0.42	0.210	9.32E28	0.331	0.253
Sun (high res) ^a	1.46	0.539	1.14E29	1.97	0.995
Sun (low res) ^a	1.46	0.563	1.34E29	1.62	0.758

^aCorresponding to the solar maximum of 2000 April 19.

^bMean surface magnetic field computed from the magnetogram.

^cMass loss rate

^dAngular momentum loss rate

^eWind ram pressure

plots of the stellar coronae complete with Alfvén Surface, wind velocity slice and magnetic field lines can be found in Figures 10 and 11, to give a clearer visualisation of simulation results. The numerical results are summarised concisely in Table 2.

4.1. Solar Analogues

The rotation periods of the stars of our sample are illustrated as a function of their ages in Figure 3. The trend shown follows the expected age-rotation relation, where the period increases as the stars get older (e.g. Gallet & Bouvier 2013). As the sample demonstrates, our study covers a significant range of rotation periods for both younger and older stars, with AB Doradus rotating with a period of only 0.5 days at a young age of 75 Myr, and HD 76151 rotating with a period of 20.5 days at an age of 3.6 Gyr. We also note that τ Boötis has a period of only 3 days (Donati et al. 2008; Fares et al. 2009) although it is thought to be fairly old at 2.4 Gyr (Saffe et al. 2005). If we look at the four stars older than 500 Myr, it is apparent that τ Boötis is indeed somewhat of an outlier for its age. However, it should be noted that this star has a hot Jupiter companion which could affect the magnetic cycle, activity and angular momentum loss (see Butler et al. 1997; Catala et al. 2007; Donati et al. 2008; Fares et al. 2009; Cohen et al. 2010b, for details). In Figure 4, we observe a decrease of magnetic field strength with age and rotation period. Since stellar magnetic dynamos are thought to be intrinsically linked to rotation (e.g. Skumanich 1972; Pallavicini et al. 1981; Wright & Drake 2011), this an

expected result (see also, e.g., Vidotto et al. 2014).

Mass and angular momentum loss rates as a function of both stellar age and rotation period are illustrated in Figures 5 and 6, respectively. Both quantities exhibit descending trends with age and rotation period, as expected. Again, τ Boötis lies above the trends for its age, by almost an order of magnitude for mass loss and two orders of magnitude for angular momentum loss, compared to the 3.6 Gyr old star HD 76151.

The bottom plot in Figure 5 illustrating the angular momentum loss rate also shows the Skumanich Law describing the decay of angular velocity with time, $\Omega \sim t^{-0.5}$, in blue and a power law fit to the data. The latter corresponds to $\Omega \sim t^{-0.36}$ in black. The older stars conform quite closely to the Skumanich relation, with the exception of τ Boötis. When removing τ Boötis from the fit, we find a relation of $\Omega \sim t^{-0.51}$ (shown in red in the bottom panel).

Figure 6 shows the stars organised by rotation period as opposed to age. We see that τ Boötis fits quite well with younger stars of comparable period for angular momentum loss rate, but yields a much lower mass loss rate. We discuss this star as an outlier in our sample in Section 5.6.

It is also known that the coronal X-ray emissions of stars correlate very well with stellar age and rotation, notably for solar type stars (see e.g. Gudel et al. (1996); Ribas et al. (2005); Guinan & Engle (2009)). X-ray emission is conspicuously greater for younger stars, as are mass and angular momentum loss rates. We thus find a consistent result when plotting these loss rates

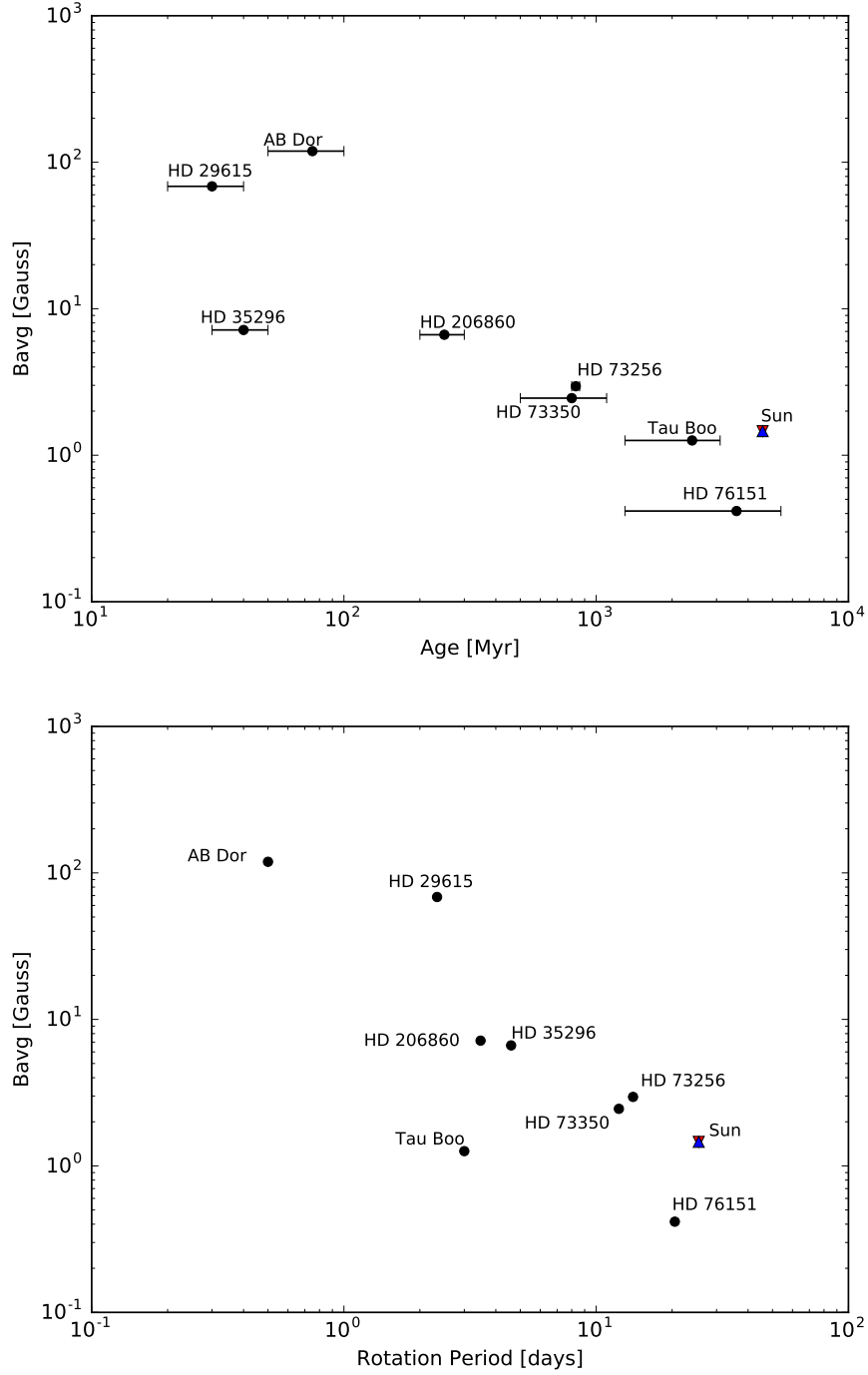


Figure 4. Plots of average surface magnetic field strength against stellar age and rotation period. The upward triangle is the high resolution solar case and the downward triangle the low resolution solar case. Note that these overlap.

against X-ray flux in Figure 7, where we see a clear correlation between the quantities.

Finally, Figure 8 illustrates the magnetospheric stand-off height of a 1 AU planet with an equatorial dipolar field strength of 0.3 G as a function of stellar age for fast and slow wind conditions. The general trend is that the magnetospheric radii grow larger as the stars grow older, reflecting the commensurate decline in wind intensity.

In the case of the for younger stars, the fast wind conditions tend to result in a larger magnetosphere, whereas the opposite is true for our sample of older stars, where the slow wind conditions yields larger magnetospheres.

Three-dimensional visualisations of the solar analogue wind conditions are shown in Figures 10 and 11. In general, the younger stars have stronger and somewhat more complex magnetic fields and faster winds than

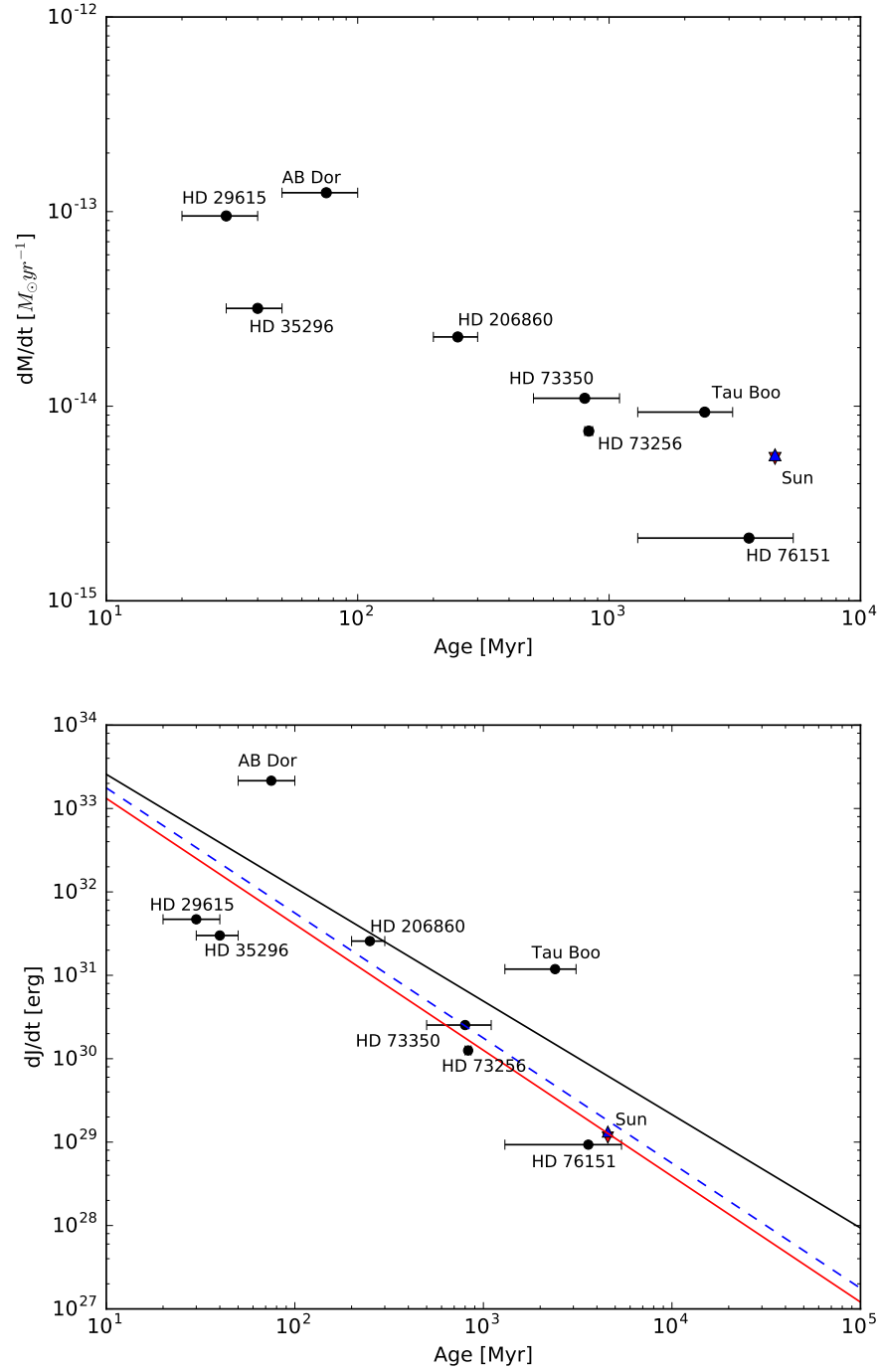


Figure 5. Plots of mass and angular momentum loss rates against stellar age. The upward triangle is the high resolution solar case and the downward triangle the low resolution solar case. In the bottom plot, the blue dashed line is the Skumanich Law, while the black line is our power law fit with $\Omega \sim t^{-0.36}$. The red line is our power law fit excluding τ Boötis with $\Omega \sim t^{-0.51}$.

the older stars. The four youngest stars, HD 29615, HD 35296, AB Doradus and HD 206860, all have maximum wind speeds that reach well over 1000 km s^{-1} , whilst the older stars HD 73350, HD 73256, τ Boötis and HD 76151 barely reach such velocities. The complexity of the magnetic field is also more important for the younger stars, which often have twisting and bending field lines, related to fast rotations as has been shown in other studies (e.g. [Cohen & Drake 2014](#)). This transitions to calmer and straighter field lines for older stars, with HD 206860 being a good example of the transitory stage. However, it should be noted that the magnetic field of τ Boötis is also quite ordered, even with a relatively rapid rotation period of 3 days. Owing to their more rapid rotation, younger stars have stronger magnetic fields and this trend is followed by the stars in our sample. In particular, the stars HD 29615 and AB Doradus have very strong fields, which are responsible for the very large sizes of their Alfvén Surfaces. The domain of the simulations had to be extended to 60 and 80 stellar radii, respectively, in order to fully encompass their Alfvén surfaces and accurately calculate mass and angular momentum loss rates.

4.2. Solar Magnetograms

The mass and angular momentum loss rates of the solar magnetograms are included in Figures 5 and 6. Immediately, it is clear that the loss rates do not depend strongly on magnetogram resolution.

The mass loss rates are found to be 5.4×10^{-15} and $6.0 \times 10^{-15} M_{\odot} \text{ yr}^{-1}$ for the high and low resolution magnetograms, respectively. These values are slightly lower than the observed value of about $2 \times 10^{-14} M_{\odot} \text{ yr}^{-1}$. The explanation for this is that solar wind MHD models typically need a factor of 2–3 applied to the input magnetograms in order to obtain the right magnitude of the magnetic flux at 1 AU ([Cohen et al. 2008](#); [Riley et al. 2012](#); [Linker et al. 2013](#)). We do not wish to apply arbitrary scaling factors to the stellar magnetograms here as the aim of our study is to examine the trends in wind conditions using only the magnetic field data as an input. We therefore choose to use a scaling factor of 1 for all maps, including the solar ones, for consistency, and as such do not expect to recover solar mass loss rates consistent with observations. Due to the lower magnetic field in the solar map, the Alfvén surface is smaller than the one we would have with a scaling factor of 2–3 and the mass loss rate is thus also reduced relative to the validated case.

For the angular momentum loss rates, we find $1.1 \times 10^{29} \text{ erg}$ and $1.3 \times 10^{29} \text{ erg}$, respectively. We also compare the solar magnetogram results to the solar analogue results. In doing so, we find that the loss rates of both solar cases follow the trends established by the

solar analogues. For the planetary magnetosphere sizes seen in Figure 8, the high resolution case yields slightly larger radii owing to smaller wind ram pressures. Both solar results follow the analogue trend, with slower stellar winds generally yielding larger magnetospheric radii.

5. DISCUSSION

We begin this section with a detailed look at the spin evolution of our sample and cool stars in general in Section 5.1, where we also present our relation of spin evolution with time. We continue by discussing the relation between magnetic activity and the Alfvén Surface in Section 5.2, followed by mass loss rate in Section 5.3. We then compare our simulation to more observation based studies in Section 5.4. We present a relation for ram pressure evolution with time in Section 5.5, and address the uniqueness of τ Boötis in Section 5.6. Finally we examine the results of the solar magnetograms in context with the analogues and compared to other studies in Section 5.7.

5.1. Rotation Period and Spin Evolution

Within the general paradigm of stellar rotation evolution in which stars spin down with age as a result of angular momentum loss through magnetized winds, younger stars have faster rotation rates and a larger spread in rotation periods ([Soderblom et al. 1993](#); [Queloz et al. 1998](#); [Bouvier et al. 2013](#); [Gallet & Bouvier 2013](#); [Johnstone et al. 2015](#); [Gallet & Bouvier 2015](#)), while older stars (around 0.3 Gyr for solar mass stars [Gallet & Bouvier 2015](#)) tend to follow the Skumanich Law $\Omega \sim t^{-1/2}$ ([Skumanich 1972](#); see however, evidence for departures from this behavior presented by [van Saders et al. 2016](#)).

Once they have shed their natal circumstellar disks that are thought to modulate rotation through “disk locking”, stars subsequently spin-up by a factor of 5–10 during their first tens of Myr (e.g. [Matt et al. 2015](#); [Gallet & Bouvier 2015](#)) as a result of the contraction and moment of inertia change that occurs during evolution to the zero-age main-sequence. The stars from our sample appear to follow this paradigm of spin evolution (see Figure 3). The rotation periods of the youngest stars in our sample are then a product of the longevity of the disk-locking phase that can negate the reduction in moment of inertia while it lasts, as well as the subsequent post-disk contraction. AB Dor is a young (75 Myr) zero-age main-sequence star that has undergone the spin up stage but has yet to spin down significantly. Since HD 29615 and HD 35296 are only 30 and 35 Myr old respectively, it is possible that they may still be in the spin-up stage, although their longer rotation periods relative to that of AB Dor could also have resulted from a

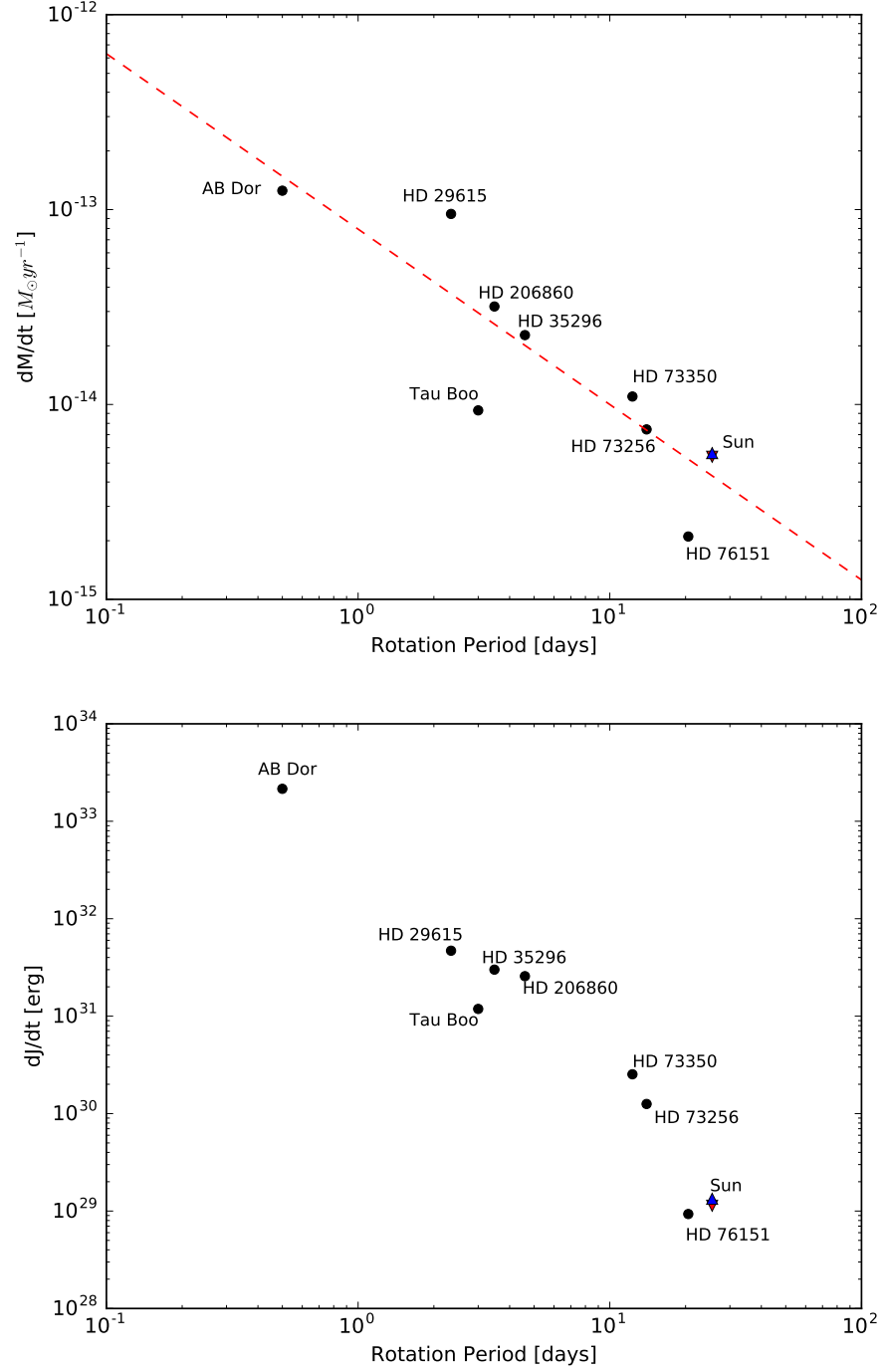


Figure 6. Plots of mass and angular momentum loss rates against rotation period. The upward triangle is the high resolution solar case and the downward triangle the low resolution solar case (note that these symbols overlap on the plot). The red line in the top plot is our fit of $dM/dt \propto P^{-0.90}$.

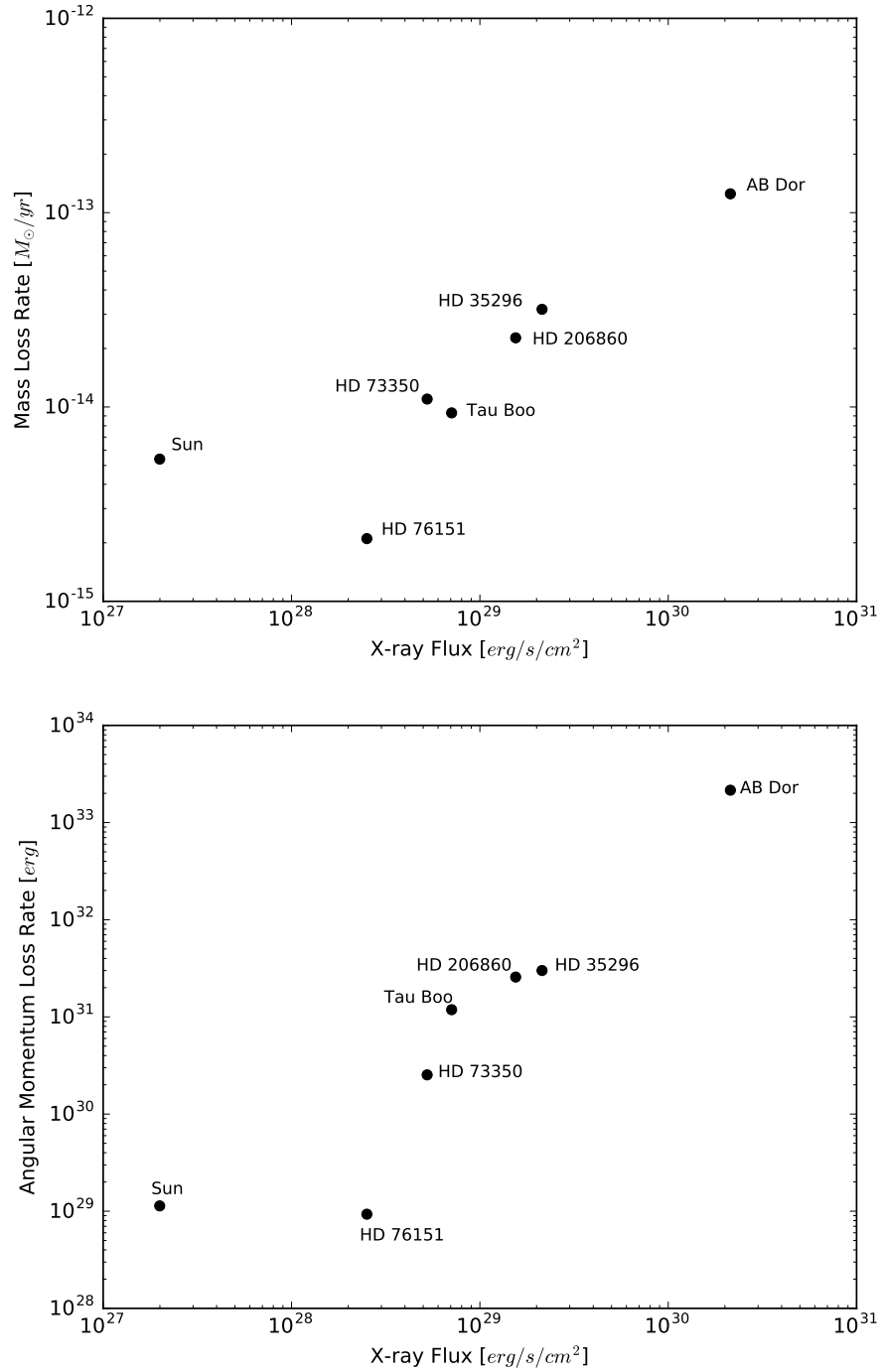


Figure 7. Plots of mass and angular momentum loss rates against coronal X-ray flux^a.

^aX-ray fluxes from [Gudel et al. \(1996\)](#) and <http://www.hs.uni-hamburg.de/DE/For/Gal/Xgroup/nexus/index.html>

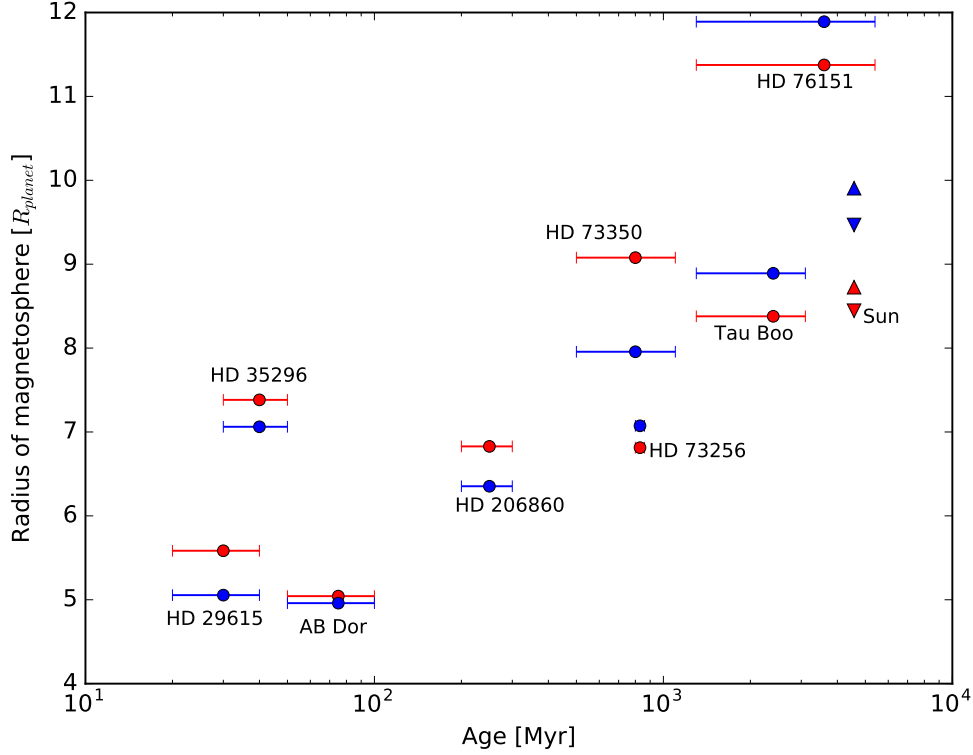


Figure 8. Plot of possible magnetospheric standoff distances for an Earth-like planet situated at 1 AU with a 0.3G equatorial magnetic field vs. stellar age. The red points represent the radius of the magnetosphere for the fastest stellar wind, and the blue points for the slowest stellar wind. The upwards triangles are the high resolution solar case and the downwards triangle the low resolution solar case.

longer disk-locking phase that stifled early spin-up.

It is now widely accepted that rotation, combined with convection, powers the magnetic dynamo, which is the driver of stellar magnetic activity (e.g. Pallavicini et al. 1981; Noyes et al. 1984; Moss 1986; Wright et al. 2011). Thus it is expected that the spin evolution of solar like stars can be used to probe the evolution of the dynamo. As the spin evolution of the star is directly related to angular momentum loss (see equation 3), it is straightforward to examine the spin evolution of our sample. Using a power law fit to the angular momentum loss rate and then integrating (see Equation 3), we find that the spin evolution goes as $\Omega \propto t^{-0.35}$, and when the apparent outlier τ Boo is removed, as $\Omega \propto t^{-0.51}$ —remarkably close to the Skumanich Law $\Omega \propto t^{-0.5}$. Considering that this law is only applicable for older stars (Skumanich 1972), and that we use a relatively small sample, it is unsurprising that the exact relation is not recovered, but encouraging that a close fit is found. This provides some support that our MHD model properly reproduces the physics driving the dynamo powered stellar winds.

5.2. Alfvén Surface and Magnetic Activity

Magnetic activity is also naturally linked to the overall strength of the magnetic field, which is ultimately re-

sponsible for driving the stellar wind. The stellar wind environment and size of the Alfvén Surface then depend on both the magnetic field strength and rotation period of the stars somewhat degenerately. The Alfvén Surface is expected to be larger for stronger fields and faster rotators (Matt et al. 2012; Cohen & Drake 2014) (see Figures 10 and 11 for visualisation). Several studies have been conducted showing that magnetic field strength has a stronger effect on the Alfvén radius, and thus angular momentum loss, than rotation rate, especially for dipolar fields (e.g. Pinto et al. 2011; Matt et al. 2012; Cohen & Drake 2014).

Cohen & Drake (2014) conducted a detailed analysis of the dependence of the Alfvén Surface, mass loss and angular momentum loss on magnetic dipole component, rotation period and base density using an MHD simulation grid. They found that the Alfvén Surface increases its overall size with both magnetic field and rotation period, and that mass loss is greater for stronger fields, which have slower but denser stellar winds. While our results agree that stronger magnetic fields yield larger mass loss rates, we find that the winds for these strong fields are faster than for the weak fields (see Figures 10 and 11). We believe these qualitative discrepancies are due to the fact that our analogue magnetograms do

not exhibit dipole-like behaviour (see Figure 1). Many studies have been conducted to show that the effect of the magnetic field is altered and reduced for more complex morphologies (see Pinto et al. 2011; Cohen & Drake 2014; Garraffo et al. 2015, for example) though it remains important as seen in our results for AB Doradus and HD 29615, which both have strong magnetic fields and Alfvén Surfaces that extend almost up to 80 and 60 stellar radii respectively.

As rotation is believed to be linked to the magnetic dynamo and thus the magnetic field, the role rotation plays for the angular momentum and mass loss rates of fast rotating young stars is of some interest. Airapetian & Usmanov (2016) find from 3D MHD simulations that for rotation periods of 2.5-25 days, rotational effects such as centrifugal force are negligible for mass loss rate and wind speed such that we can conclude that rotation period dependencies in our results are due to its influence on the attendant magnetic field. Stronger magnetic fields in the absence of other changes in wind parameters will lead to larger Alfvén surfaces and so increased angular momentum loss rates. Greater Poynting flux from stronger magnetic field is also expected to drive more mass loss, which acts to decrease the Alfvén surface size. The interplay between the two effects can be complex—see, e.g., the discussion of Matt et al. (2012) for the case of Parker-type winds.

5.3. Mass Loss Rate

We see from our results (see Figures 4 and 6) that the mass loss rate is anticorrelated with rotation period. In order to compare stars of different spectral type, rotation is often expressed in terms of the Rossby number, defined as $Ro = P_{rot}/\tau_c$, where P_{rot} is the rotation period and τ_c is the convective turnover time. Recently, a study conducted by See et al. (2017) used a potential field source-surface model to approximate MHD calculations of angular momentum and mass loss rates on 66 ZDI mapped solar analogues as a function of Rossby number. They find that the loss rates decrease with Rossby number as expected, with angular momentum rates similar to our results, but with mass loss rates which are acknowledged as being too high. Aside from the general trends expected, See et al. (2017) also make note of a saturated loss rate regime for low Rossby numbers ($Ro < 0.1$; see also Sadeghi Ardestani et al. (2017)) that coincides with the general magnetic saturation seen through the magnetic activity diagnostic of X-ray emission (e.g. Wright et al. 2011). Wright et al. (2011) found saturation limits in terms of both an empirical Rossby number as well as rotation period; the latter as a function of stellar mass. For solar mass stars, the convective turnover time is about 20 days, and saturation occurs at a rotation period of 2.6 days. Of our sample, AB Dor

is clearly in the saturated regime, but the remainder are either at the saturated-unsaturated limit (HD 29615) or else are unsaturated. It would be interesting in future studies to include faster rotators to probe the early spin-down phase of solar mass stars and explore further the magnetically saturated wind regime and mass loss saturation effects found by See et al. (2017).

The mass loss rates found in this study are between $10^{-12} - 10^{-15} M_{\odot}/yr$, an order of magnitude lower than the range presented in most studies (e.g Cranmer & Saar 2011; Airapetian & Usmanov 2016; See et al. 2017). This potential discrepancy is explained due to our omission of magnetic field scaling of the ZDI magnetograms, as explained in Section 4.2. When looking at the mass loss rates as a function of age, it is interesting to compare our results to those found in other MHD simulations such as Airapetian & Usmanov (2016), and those found in theoretical models such as that of Cranmer & Saar (2011). It is reassuring that the results of Airapetian & Usmanov (2016) agree with our simulation results, excepting the order of magnitude for mass loss rates. Furthermore, these values are also consistent with the study of Wood et al. (2005), which were based on observations of Ly α absorption in stellar “astrospheres” (see Section 5.4). However, Airapetian & Usmanov (2016) only take their simulations back to 0.7Gyr, whereas Cranmer & Saar (2011) use a physically motivated model for the winds of cool stars, and cover a range of ages down to 1Myr. The models presented in that work follow turbulent MHD motion from stellar convective zones driven by gas pressure for solar like stars relevant to our study. Cranmer & Saar (2011) present a mass loss rate model as a function of age covering the entire range of our sample, which is very consistent with the trends we see from our mass loss rates, including the young “spin-up” phase for stars between 10 – 50 Myr.

We can also compare our simulation results to semi-empirical works. Johnstone et al. (2015) studied the wind and mass loss evolution of sun-like stars, while Sadeghi Ardestani et al. (2017) adopted a semi-empirical model approach, both in an attempt to build a general spin down model for stars of ages ranging from 10 Myr to 4 Gyr. Both use the wind torque relation derived in Matt et al. (2012), finding a relation for mass loss rate to stellar mass, radius and rotation, though the semi-empirical model also factors in mixing time for angular momentum transfer inside the stellar envelope. Comparing their qualitative results of mass loss evolution to the trends found from our study, we again see the same general evolution that mass loss rate decreases with age and as rotation period increases. However, they find a steeper slope for these relations than our results, with $dM/dt \propto P^{-1.33}$ (Johnstone et al. 2015), and $dM/dt \propto P^{-1.3}$ (Sadeghi Ardestani et al. 2017), where

P is rotation period, while we find $dM/dt \propto P^{-0.90}$.

5.4. X-ray and Indirect Mass Loss Rate Observations

X-ray and extreme ultraviolet (EUV) emission are often used to probe stellar magnetic activity (Gudel et al. 1996; Ribas et al. 2005; Guinan & Engle 2009), with X-ray saturation being of particular interest (Wright et al. 2011; See et al. 2017). From our results in Figure 7, it is difficult to see a saturated X-ray regime due to the small sample. However, we clearly see that the mass and angular momentum loss rates appear closely correlated to the X-ray flux. This is due to the fact that all these quantities are indicators of the magnetic dynamo's activity. This does not indicate that one is the causation of the others. For example, Cohen (2011) has found that the Sun's mass loss rate stays at an average of $2 \times 10^{-14} M_{\odot}/yr$ without following the variations of solar X-ray flux. This is explained by the mass loss rate being heavily dependent on stable open magnetic flux, while X-ray emission also depends on the more variable closed magnetic flux. Since X-ray flux correlates well with magnetic activity, it also correlates very well with Rossby number, defined as rotation period divided by convective turnover time τ . Thus if τ is known for a certain spectral type, rotation period can be inferred, albeit with some uncertainty, from X-ray luminosity, and using gyrochronology for stars older than $\sim 1\text{Gyr}$, age can be inferred. However, this method has some flaws which have been detailed, notably that this method is difficult to apply for younger stars, and that there exists a large spread of ages for a certain rotation period (Barnes 2003; Barnes & Kim 2010). Since we already take into account uncertainty in our sample's ages and rotation periods, and there are also some disagreements for the spectral types in literature, we omit any derivation of our sample's ages using X-ray flux.

Wood et al. (2005, 2014, 2015) indirectly measured the mass loss rates for cool main sequence stars using absorption in high dispersion spectra of $\text{Ly}\alpha$ 1215.7 Angstrom in stellar astrospheres. The general trends observed here are consistent with those found in this work, notably that mass loss rate decreases with age and the values sit in an interval between 10^{-12} to 10^{-14} solar masses per year. However, Wood et al. (2015) suggest that young stars with ages less than 0.7Gyr may in fact have weaker winds more akin to those of the Sun, rather than the powerful winds inferred from the high mass loss rates in this work. The star π^1 UMa is taken as an example. This is a G1.5 spectral type star, with an age of $\sim 300\text{Myr}$ and rotation period of ~ 5 days, similar to HD 206860 in our sample. While we find a mass loss rate for HD 206860 an order of magnitude higher than for the Sun, Wood et al. (2015) find a value for π^1 UMa lower than for the Sun. This may be explained in

terms of the complexity of the magnetic field. The π^1 UMa detection is very interesting in the context of the current discussion on young stars' spin-down. There is increasing evidence indicating that young, active stars can store larger fractions of their magnetic flux in higher order spherical harmonics (Donati et al. 2008; Donati & Landstreet 2009) which they lose as they age. This complexity should lead to a suppression of dM/dt and angular momentum loss (Réville et al. 2015a,b; Garraffo et al. 2015, 2016). These results combined may indicate that very active stars suffer a suppression of mass loss rates due to magnetic field complexity. The bimodal distribution of rotation periods in open cluster observations suggest that for any age, there are some stars that behave like dipoles and some that behave like more complex morphologies not losing angular momentum or mass at an efficient rate. HD 206860 does not show a very complex field, either due to the lack of sensitivity of the ZDI technique or perhaps this star's complexity has already evolved towards a simpler one. Such a dispersion in dM/dt values might then be naturally expected for young stars.

In summary, the overall trends here established by the solar analogue sample are as expected and generally agree with previous studies.

5.5. Planetary Magnetosphere Evolution

The results obtained for the range of planetary magnetosphere sizes also confirm the expected trend of an increase in size as stars age, since weaker winds will exert less ram pressure. The size of the magnetosphere depends on the pressure exerted by the stellar wind, which in turn is related on the velocity and density of the wind. When probing the densities and velocities of the stellar winds, we find that the slower winds consistently have a higher density. A switch occurs in which winds density is a more dominant factor in the ram pressure than velocity for younger stars, while the opposite is true for older stars.

Using the wind velocity and density results, we fit a power law relation to the mean of the minimum and maximum ram pressures listed in Table 1 as a function of age. By scaling this relation with orbital distance, we can then derive a relationship that describes the evolution of the wind ram pressure throughout the solar system as a function of time:

$$\overline{P}_{ram} = 6.10 \times 10^{-7} t^{-0.67} / r^2 \quad (5)$$

where t is age in Myr and r is distance in Au. This is illustrated as a set of loci corresponding to the pressure as a function of orbital radius for different ages in Figure 9. As expected, the ram pressure decreases with age, consistent with the star spinning down and the stellar

winds undergoing a steady secular loss in power. This is in agreement with previous studies that have found that the solar wind pressure at Earth’s magnetopause was much greater in the past, potentially up to two orders of magnitude between present day Gyr ages and early ~ 10 Myr ages (Sternberg et al. 2011; Airapetian & Usmanov 2016).

5.6. *Tau Boötis as a Potential Outlier*

Of the eight solar analogues examined in this study, τ Boötis stands out the most as a potential outlier. In Figure 3, we see that τ Boötis rotates at a much faster rate than any of the other stars of comparable age, with a rotation period of merely 3 days. Since it is generally accepted that rotation is responsible for powering the magnetic dynamo, one would expect the average surface magnetic field strength to be more akin to those of the young, fast rotators. Figure 4 clearly shows that this is not the case, and indeed τ Boötis fits very well with stars of similar ages, even when they are rotating much slower. Indeed, its mean surface magnetic field is found to be 1.26 G, while comparable rotators HD 29615 and HD 35296 with 2.32 and 3.9 day periods both have much larger average magnetic fields of 119 G and 68.5 G respectively. As such, with a rotation period of 3 days, one could expect to have an average field strength somewhere between these two values.

τ Boötis’ angular momentum loss rate places it comfortably with the young stars, but its mass loss rate places it more with the old stars of our sample (see Figures 5 and 6). Since angular momentum loss rate is directly proportional to angular frequency (see equation 2), it is unsurprising that τ Boötis fits well with other young rotators. However, mass loss rate (see equation 1) depends only on the wind velocity at the Alfvén Surface and the wind density. Furthermore, as discussed in Section 5.1, when removing τ Boötis from the fit shown in Figure 5, we find a relation $\Omega \sim t^{-0.51}$ (shown in red in the bottom panel), which is even closer to the Skumanich Law than when τ Boötis is included in the fit (which yields $\Omega \sim t^{-0.36}$). While this should not be used as support for treating this particular star as an outlier, that the spin-down relation moves in the direction toward that observed is encouraging.

There are several reasons that could seek to explain why the τ Boötis results appear to be so out of place. As mentioned in Section 3.7, τ Boötis is host to a hot Jupiter with an orbital period of 3.3 days with potentially strong tidal effects (Butler et al. 1997; Catala et al. 2007; Donati et al. 2008; Fares et al. 2009). The magnetic field of the giant planet may also interfere with that of the star, further altering the results derived from our simulations. Furthermore, there are large uncertainties on the age of τ Boötis, with values generally ranging

between 1.3-2.1 Gyr (see Section 3.7). Thus it is possible that τ Boötis is in fact a true outlier for physical reasons.

There may also be technical reasons behind the apparent uniqueness of the τ Boötis results. It was noted during its spectropolarimetric observations that “the Zeeman signatures of τ Boo are extremely small,” (Fares et al. 2009) which could account for the weak field magnitude relative to its rotation rate. Furthermore, we see in Figure 1 that the map for τ Boötis appears to be of poor quality relative to the others and it is possible that the ZDI-derived magnetogram is flawed. We also note that Vidotto et al. (2012) conducted a similar wind model study on τ Boötis and found loss rates of $2.7 \times 10^{-12} M_{\text{sol}}$ per year and $1.5 \times 10^{32} \text{ erg}$. These results are 2 and 1 orders of magnitude above our already high results, though are based on less physically realistic Parker-type winds.

In summary, until additional ZDI observations of τ Boötis are acquired and the present results can be verified they should be treated with caution.

5.7. *Solar Results in Context*

In order to investigate how the case of the Sun fits in with the results for the solar analogues it is interesting to bring the two solar magnetogram results into the picture. Figures 4, 5 and 6 show these results as upwards and downwards triangles for the high and low resolution magnetograms respectively. It is clear that the difference in resolution does not appear to change the results much, as the magnetic field strength and loss rates are essentially identical. As noted earlier, both high and low resolution cases fit the analogue trend. For the mass loss rates, Sternberg et al. (2011) reported a rate of 4.28×10^{-14} solar masses per year for the same high resolution magnetogram, while the solar wind study by Cohen (2011) found that the average mass loss rate of the Sun is about 2×10^{-14} solar masses per year. Our mass loss rate is 5.7×10^{-15} solar masses per year—slightly lower than found in other studies. As mentioned in Section 4.2, we chose to not apply the 2–3 multiplicative correction to the input magnetograms’ magnetic fields, which are needed to obtain the right magnitude of the magnetic flux at 1 AU (Cohen et al. 2008; Riley et al. 2012; Linker et al. 2013), in order to avoid arbitrary scaling of data. Since we did not rescale any magnetic maps, finding a lower mass loss rate for the Sun relative to the validated case is expected.

The inclusion of two different resolution solar magnetograms in this study also serves to test the accuracy of ZDI maps and to address the question of whether small-scale features such as spots could significantly influence mass and angular momentum loss rates. It has been shown that for an underlying dipolar field morphol-

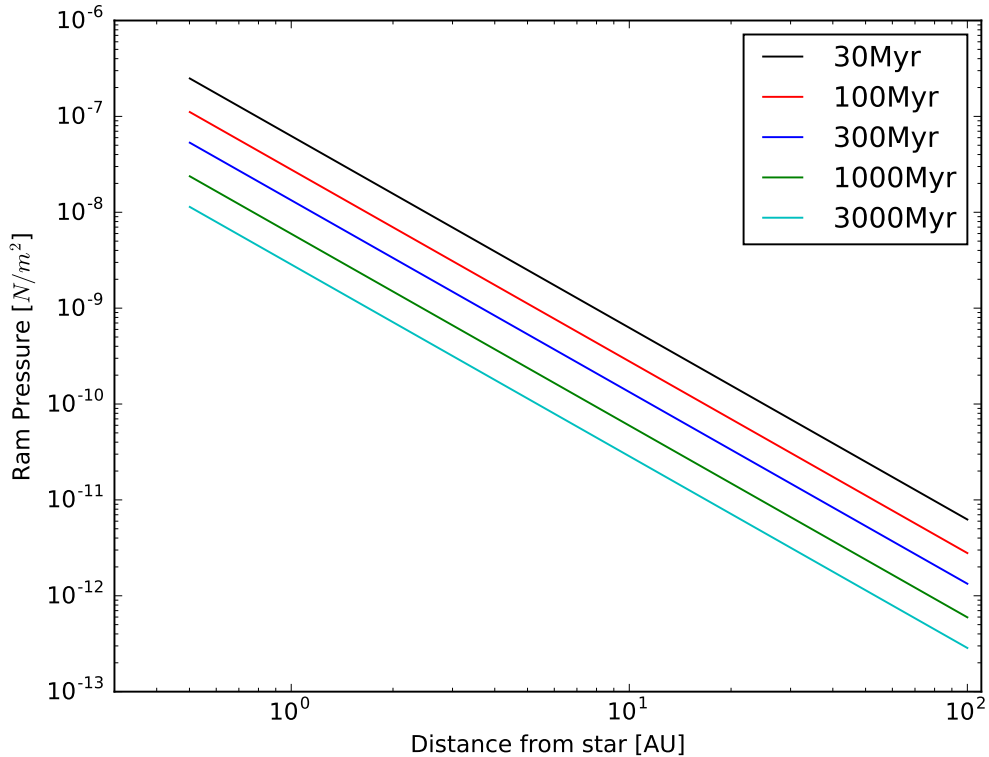


Figure 9. Plot of ram pressure with distance at loci of different ages.

ogy, the large scale structure dominates smaller features such as sunspots in controlling wind properties (Garraffo et al. 2013). The Sun is not a dipole during solar maxima, thus allowing the influence of small scale features to be tested. We find that the difference in resolution between the MDI and WSO observations is insignificant for the purposes of predicting the wind global properties.

Several previous studies have simplified the problem of magnetic field morphology by assuming purely dipolar fields when simulating the younger Sun (e.g. Matt et al. 2012; Cohen & Drake 2014; Matt et al. 2015; Airapetian & Usmanov 2016). It is not known what the underlying magnetic morphology of solar analogues is in general and the magnetograms in Figure 1 are not clearly indicative of dipoles. Field morphology also likely changes through the lifetime of the star (e.g. Garraffo et al. 2015). This must be kept in mind when placing this work in context with other studies, especially since dipolar fields were shown by (e.g. Garraffo et al. 2015) to be more efficient at removing mass and angular momentum from the star than multipole fields. Furthermore, ZDI is easiest to apply to bright, nearby, fast-rotating stars exhibiting both stronger magnetic field and Doppler signatures (Donati & Brown 1997). As such, the younger and faster rotating stars of our sample are generally expected to have better data quality than the much older and more slowly rotating stars. This could potentially induce a bias into

the results. That this is probably not a serious effect is supported by the trends obtained from ZDI magnetic maps by Vidotto et al. (2014) that agree with expectations of the evolution of magnetic activity with age, and by the fact that our solar analogue sample reproduces a Skumanich-like spin-down trend.

Considering the solar analogues truly as proxies for a younger Sun, we find that the general trends established are consistent with previous studies employing many various models for mass loss and spin evolution of the Sun (e.g. Cranmer & Saar 2011; Johnstone et al. 2015; Airapetian & Usmanov 2016; Sadeghi Ardestani et al. 2017; See et al. 2017).

6. CONCLUSIONS

A sufficient body of magnetic maps of solar analogues now exists with which to perform detailed numerical simulations that can be used to investigate the history of the Sun and solar system interplanetary environment.

A state-of-the-art 3-D MHD model of the solar wind based on the dissipation of Alfvén wave turbulence has been applied to a sample of eight solar-like stars with a range of ages and activity levels. The only variable in the model input was the spatially-dependent radial magnetic field at the lower boundary. Test case solar simulations employed lower resolution WSO and high resolution MDI magnetograms, while stellar simulations used

magnetograms derived from Zeeman-Doppler imaging.

Both angular momentum and mass loss rates derived from the simulations decrease with stellar age, as expected. From the angular momentum loss rates we derived the spin down rate and find that angular velocity decreases with time according to $\Omega \propto t^{-0.36}$. When omitting one outlier star, the planet hosting τ Boo, whose magnetogram, magnetic and rotation properties appear anomalous, the spin-down relation is described by $\Omega \propto t^{-0.51}$. This is remarkably similar to the Skumanich relation $\Omega \propto t^{-0.5}$.

The difference in spatial resolution between MDI and WSO solar magnetograms does not lead to significant differences in the solar wind simulation results.

The simulation results were used to compute the wind ram pressure for each stellar case. This was used to investigate the magnetospheric stand-off distance for an Earth like planet with an equatorial magnetic field strength of 0.3 G situated at 1 AU. At early times of a few tens to a hundred million years, such a magnetosphere would have been compressed to half of its present-day extension. An expression for the the wind ram pressure as a function of radial distance and time was derived that indicates that solar wind pressure has declined by a factor of about 50 since the Sun reached

the zero-age main-sequence.

With improvements in ZDI observational methods and in capabilities of the model, future data should allow for the Sun's history to be simulated even more realistically through the use of Sun-like stars as solar proxies.

We would like to thank our anonymous referee for a very thorough and constructive review of our work. QP thanks the High Energy Astrophysics Division of the Harvard-Smithsonian Center for Astrophysics for accommodating him on such a project. This work was carried out using the SWMF/BATSRUS tools developed at The University of Michigan Center for Space Environment Modeling (CSEM) and made available through the NASA Community Coordinated Modeling Center (CCMC). The simulations were performed on the SI Hydra cluster. CG acknowledges support from the NASA Living with a Star program grant NNX16AC11G. JJD was funded by NASA contract NAS8-03060 to the *Chandra X-ray Center* and thanks the Director, Belinda Wilkes, for continuing support.

REFERENCES

- Airapetian, V. S., Carpenter, K., & Ofman, L. 2003, in *Bulletin of the American Astronomical Society*, Vol. 35, American Astronomical Society Meeting Abstracts #202, 745
- Airapetian, V. S., & Usmanov, A. V. 2016, *ApJL*, 817, L24
- Alvarado-Gómez, J. D., Cohen, O., Hussain, G. A. J., et al. 2015, in *IAU Symposium*, Vol. 305, *Polarimetry*, ed. K. N. Nagendra, S. Bagnulo, R. Centeno, & M. Jesús Martínez González, 282–287
- Alvarado-Gómez, J. D., Hussain, G. A. J., Cohen, O., et al. 2016, *A&A*, 588, A28
- Barnes, S. A. 2003, *ApJ*, 586, 464
- . 2007, *ApJ*, 669, 1167
- Barnes, S. A., & Kim, Y.-C. 2010, *ApJ*, 721, 675
- Belcher, J. W. 1971, *ApJ*, 168, 509
- Bonanno, A., Schlattl, H., & Paternò, L. 2002, *A&A*, 390, 1115
- Boothroyd, A. I., & Sackmann, I.-J. 2003, *ApJ*, 583, 1004
- Boro Saikia, S., Jeffers, S. V., Petit, P., et al. 2015, *A&A*, 573, A17
- Borsa, F., Scandariato, G., Rainer, M., et al. 2015, *A&A*, 578, A64
- Bouvier, J., Matt, S. P., Mohanty, S., et al. 2013, *ArXiv e-prints*, arXiv:1309.7851
- Brown, S. F., Donati, J.-F., Rees, D. E., & Semel, M. 1991, *A&A*, 250, 463
- Butler, R. P., Marcy, G. W., Williams, E., Hauser, H., & Shirts, P. 1997, *ApJL*, 474, L115
- Catala, C., Donati, J.-F., Shkolnik, E., Bohlender, D., & Alecian, E. 2007, *MNRAS*, 374, L42
- Claret, A., & Gimenez, A. 1989, *A&AS*, 81, 37
- Cohen, O. 2011, *MNRAS*, 417, 2592
- Cohen, O., & Drake, J. J. 2014, *ApJ*, 783, 55
- Cohen, O., Drake, J. J., Kashyap, V. L., Hussain, G. A. J., & Gombosi, T. I. 2010a, *ApJ*, 721, 80
- Cohen, O., Drake, J. J., Kashyap, V. L., Sokolov, I. V., & Gombosi, T. I. 2010b, *ApJL*, 723, L64
- Cohen, O., Drake, J. J., & Kóta, J. 2012, *ApJ*, 760, 85
- Cohen, O., Sokolov, I. V., Roussev, I. I., & Gombosi, T. I. 2008, *Journal of Geophysical Research (Space Physics)*, 113, A03104
- Connelly, J. N., Bizzarro, M., Krot, A. N., et al. 2012, *Science*, 338, 651
- Cox, A. N., & Guzik, J. A. 1995, in *Astronomical Society of the Pacific Conference Series*, Vol. 76, *GONG 1994. Helio- and Astro-Seismology from the Earth and Space*, ed. R. K. Ulrich, E. J. Rhodes, Jr., & W. Dappen, 184
- Cranmer, S. R., & Saar, S. H. 2011, *ApJ*, 741, 54
- Cranmer, S. R., & van Ballegooijen, A. A. 2005, *ApJS*, 156, 265
- De Beck, E., Decin, L., de Koter, A., et al. 2010, *A&A*, 523, A18
- Donati, J.-F., & Brown, S. F. 1997, *A&A*, 326, 1135
- Donati, J.-F., & Landstreet, J. D. 2009, *ARA&A*, 47, 333
- Donati, J.-F., Morin, J., Delfosse, X., et al. 2009, in *American Institute of Physics Conference Series*, Vol. 1094, 15th Cambridge Workshop on Cool Stars, Stellar Systems, and the Sun, ed. E. Stempels, 130–139
- Donati, J.-F., Moutou, C., Farès, R., et al. 2008, *MNRAS*, 385, 1179
- Douglas, S. T., Agüeros, M. A., Covey, K. R., Cargile, P. A., Barclay, T., Cody, A., Howell, S. B., & Kopytova, T. 2016, *ApJ*, 822, 47
- Fares, R., Moutou, C., Donati, J.-F., et al. 2013, *MNRAS*, 435, 1451
- Fares, R., Donati, J.-F., Moutou, C., et al. 2009, *MNRAS*, 398, 1383

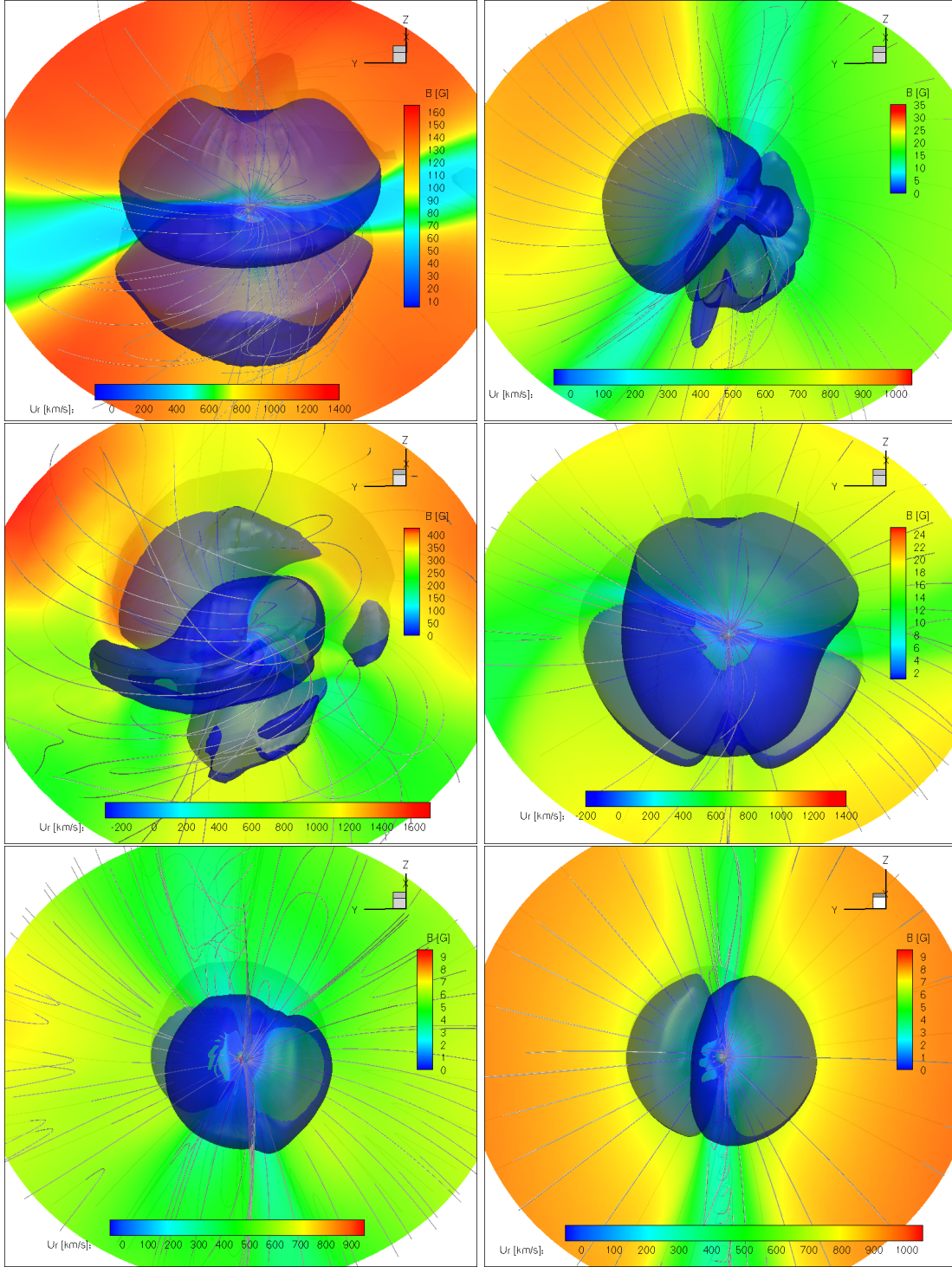


Figure 10. Three-dimensional visualisations of the first six simulation solutions, in order of ascending age from top left to bottom right: HD 29615, HD 35296, AB Dor, HD 206860, HD73350 and HD 73256. The two-dimensional contour pattern represents a slice from the radial wind velocity. The streamlines represent the magnetic field lines. The translucent surface is the Alfvén surface. The sphere at the center of the plot is the surface of the star and is flooded to show magnetic field strength. In cases where the surface is hard to see, the legend for magnetic field strength is still included to give an idea of the range of magnetic field strength involved.

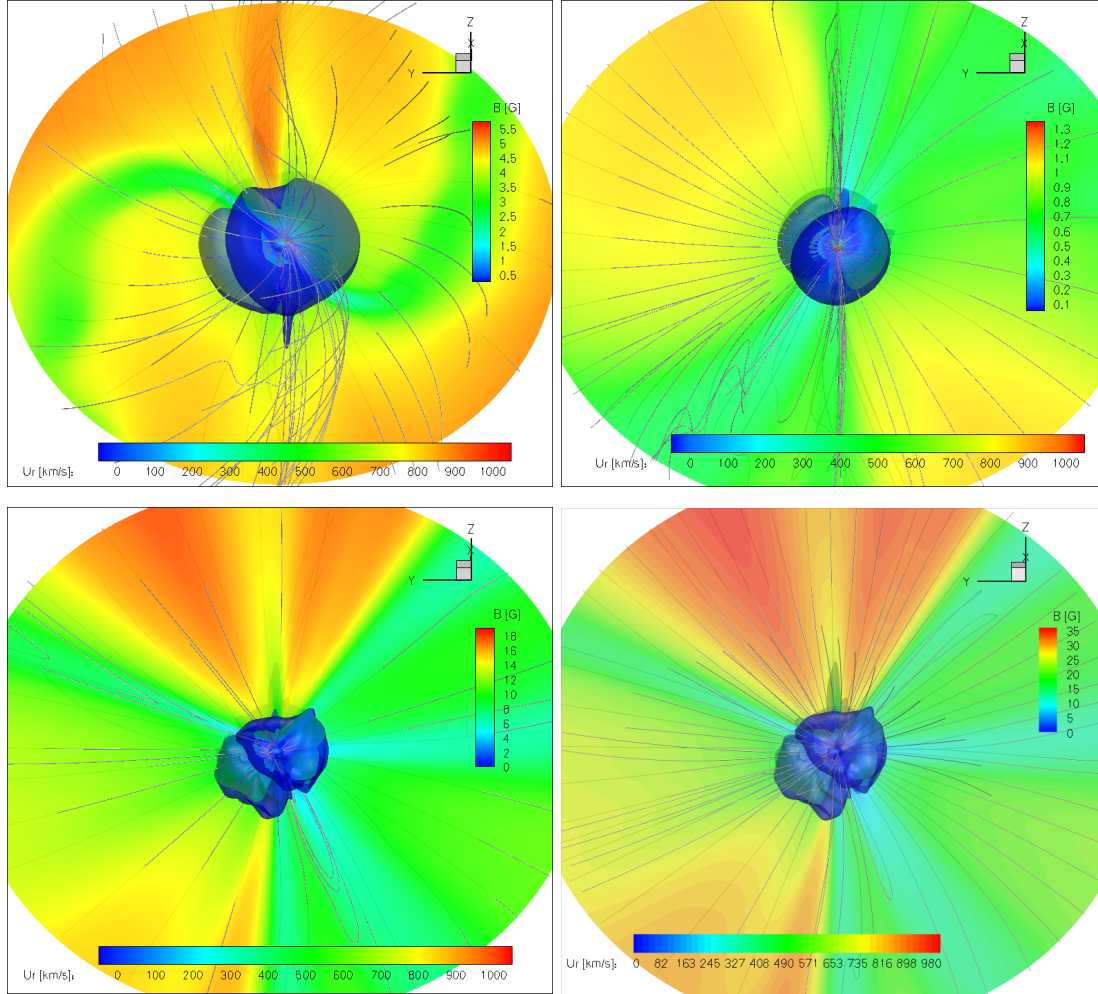


Figure 11. Three-dimensional visualisations of the four last simulation solutions in order of ascending age from top left to bottom right: Tau Boo, HD 76151, high resolution solar, low resolution solar. The two-dimensional contour pattern represents a slice from the radial wind velocity. The streamlines represent the magnetic field lines. The translucent surface is the Alfvén surface. The sphere at the center of the plot is the surface of the star and is flooded to show magnetic field strength. In cases where the surface is hard to see, the legend for magnetic field strength is still included to give an idea of the range of magnetic field strength involved.

- Fuhrmann, K., Pfeiffer, M. J., & Bernkopf, J. 1998, *A&A*, 336, 942
- Gallet, F., & Bouvier, J. 2013, *A&A*, 556, A36
- . 2015, *A&A*, 577, A98
- Garraffo, C., Cohen, O., Drake, J. J., & Downs, C. 2013, *ApJ*, 764, 32
- Garraffo, C., Drake, J. J., & Cohen, O. 2015, *ApJ*, 813, 40
- . 2016, *A&A*, 595, A110
- Güdel, M. 2007, *Living Reviews in Solar Physics*, 4, 3
- Güdel, M., Guinan, E. F., & Skinner, S. L. 1996, in *Astronomical Society of the Pacific Conference Series*, Vol. 109, *Cool Stars, Stellar Systems, and the Sun*, ed. R. Pallavicini & A. K. Dupree, 607
- Guinan, E. F., & Engle, S. G. 2009, in *IAU Symposium*, Vol. 258, *The Ages of Stars*, ed. E. E. Mamajek, D. R. Soderblom, & R. F. G. Wyse, 395–408
- Hussain, G. A. J., Jardine, M., Donati, J.-F., et al. 2007, *MNRAS*, 377, 1488
- Hussain, G. A. J., Collier Cameron, A., Jardine, M. M., et al. 2009, *MNRAS*, 398, 189
- Hussain, G. A. J., Alvarado-Gómez, J. D., Grunhut, J., et al. 2016, *A&A*, 585, A77
- Johstone, C. P., Güdel, M., Brott, I., & Lüftinger, T. 2015, *ArXiv e-prints*, arXiv:1503.07494
- Linker, J. A., Mikić, Z., Riley, P., et al. 2013, *Solar Wind* 13, 1539, 26
- Luhman, K. L., Patten, B. M., Marengo, M., et al. 2007, *ApJ*, 654, 570
- Mamajek, E. E., & Hillenbrand, L. A. 2008, *ApJ*, 687, 1264
- Matt, S. P., Brun, A. S., Baraffe, I., Bouvier, J., & Chabrier, G. 2015, *ApJL*, 799, L23
- Matt, S. P., MacGregor, K. B., Pinsonneault, M. H., & Greene, T. P. 2012, *ApJL*, 754, L26
- Meibom, S., Mathieu, R. D., Stassun, K. G., Liebesny, P., & Saar, S. H. 2011, *ApJ*, 733, 115
- Mestel, L. 1968, *MNRAS*, 138, 359
- Mestel, L., & Spruit, H. C. 1987, *MNRAS*, 226, 57
- Moss, D. 1986, *PhR*, 140, 1
- Noyes, R. W., Weiss, N. O., & Vaughan, A. H. 1984, *ApJ*, 287, 769
- Oran, R., van der Holst, B., Landi, E., et al. 2013, *ApJ*, 778, 176
- Owen, J. E., & Wu, Y. 2016, *ApJ*, 817, 107
- Pallavicini, R., Peres, G., Serio, S., et al. 1981, *ApJ*, 247, 692
- Petit, P., Dintrans, B., Solanki, S. K., et al. 2008, *MNRAS*, 388, 80
- Pevtsov, A. A., Fisher, G. H., Acton, L. W., et al. 2003, *ApJ*, 598, 1387
- Pinto, R. F., Brun, A. S., Jouve, L., & Grappin, R. 2011, *ApJ*, 737, 72
- Pizzolato, N., Maggio, A., Micela, G., Sciortino, S., & Ventura, P. 2003, *A&A*, 397, 147
- Plavchan, P., Werner, M. W., Chen, C. H., et al. 2009, *ApJ*, 698, 1068
- Powell, K. G., Roe, P. L., Linde, T. J., Gombosi, T. I., & Zeeuw, D. L. D. 1999, *Journal of Computational Physics*, 154, 284 .
<http://www.sciencedirect.com/science/article/pii/S002199919996299X>
- Queloz, D., Allain, S., Mermilliod, J.-C., Bouvier, J., & Mayor, M. 1998, *A&A*, 335, 183
- Réville, V., Brun, A. S., Matt, S. P., Strugarek, A., & Pinto, R. F. 2015a, *ApJ*, 798, 116
- Réville, V., Brun, A. S., Strugarek, A., et al. 2015b, *ApJ*, 814, 99
- Ribas, I., Guinan, E. F., Güdel, M., & Audard, M. 2005, *ApJ*, 622, 680
- Ribas, I., Porto de Mello, G. F., Ferreira, L. D., et al. 2010, *ApJ*, 714, 384
- Riley, P., Linker, J. A., Lionello, R., & Mikić, Z. 2012, *Journal of Atmospheric and Solar-Terrestrial Physics*, 83, 1
- Sadeghi Ardestani, L., Guillot, T., & Morel, P. 2017, *ArXiv e-prints*, arXiv:1709.03054
- Saffe, C., Gómez, M., & Chavero, C. 2005, *A&A*, 443, 609
- Sagan, C., & Mullen, G. 1972, *Science*, 177, 52
- Schatzman, E. 1962, *Annales d'Astrophysique*, 25, 18
- Scherrer, P. H., Bogart, R. S., Bush, R. I., et al. 1995, *SoPh*, 162, 129
- See, V., Jardine, M., Vidotto, A. A., et al. 2017, *MNRAS*, 466, 1542
- Skumanich, A. 1972, *ApJ*, 171, 565
- Soderblom, D. R., Stauffer, J. R., MacGregor, K. B., & Jones, B. F. 1993, *ApJ*, 409, 624
- Sokolov, I. V., van der Holst, B., Oran, R., et al. 2013, *ApJ*, 764, 23
- Sterenborg, M. G., Cohen, O., Drake, J. J., & Gombosi, T. I. 2011, *Journal of Geophysical Research (Space Physics)*, 116, A01217
- Suzuki, T. K. 2006, *ApJL*, 640, L75
- Terada, N., Kulikov, Y. N., Lammer, H., et al. 2009, *Astrobiology*, 9, 55
- Torres, C. A. O., Quast, G. R., da Silva, L., et al. 2006, *A&A*, 460, 695
- Tóth, G., van der Holst, B., Sokolov, I. V., et al. 2012, *Journal of Computational Physics*, 231, 870
- Udry, S., Mayor, M., Clausen, J. V., et al. 2003, *A&A*, 407, 679
- Valenti, J. A., & Fischer, D. A. 2005, *VizieR Online Data Catalog*, 215
- van Ballegooijen, A. A., Asgari-Targhi, M., Cranmer, S. R., & DeLuca, E. E. 2011, *ApJ*, 736, 3
- van der Holst, B., Sokolov, I. V., Meng, X., et al. 2014, *ApJ*, 782, 81
- van Saders, J. L., Ceillier, T., Metcalfe, T. S., et al. 2016, *Nature*, 529, 181
- Vidotto, A. A., Fares, R., Jardine, M., et al. 2012, *MNRAS*, 423, 3285
- Vidotto, A. A., Gregory, S. G., Jardine, M., et al. 2014, *MNRAS*, 441, 2361
- Waite, I. A., Marsden, S. C., Carter, B. D., et al. 2015, *MNRAS*, 449, 8
- Weber, E. J., & Davis, Jr., L. 1967, *ApJ*, 148, 217
- Wood, B. E., Linsky, J. L., & Güdel, M. 2015, in *Astrophysics and Space Science Library*, Vol. 411, *Characterizing Stellar and Exoplanetary Environments*, ed. H. Lammer & M. Khodachenko, 19
- Wood, B. E., Müller, H.-R., Redfield, S., & Edelman, E. 2014, *ApJL*, 781, L33
- Wood, B. E., Müller, H.-R., Zank, G. P., Linsky, J. L., & Redfield, S. 2005, *ApJL*, 628, L143
- Wright, N., & Drake, J. 2011, in *The X-ray Universe 2011*, ed. J.-U. Ness & M. Ehle, 171
- Wright, N. J., Drake, J. J., Mamajek, E. E., & Henry, G. W. 2011, *ApJ*, 743, 48
- Zuckerman, B., & Song, I. 2004, *ARA&A*, 42, 685